JVI Journals.ASM.org

Macropinocytosis Is the Entry Mechanism of Amphotropic Murine Leukemia Virus

Izabela Rasmussen, Frederik Vilhardt

Department of Cellular and Molecular Medicine, Faculty of Health Sciences, Copenhagen University, Copenhagen, Denmark

ABSTRACT

The entry mechanism of murine amphotropic retrovirus (A-MLV) has not been unambiguously determined. We show here that A-MLV is internalized not by caveolae or other pinocytic mechanisms but by macropinocytosis. Thus, A-MLV infection of mouse embryonic fibroblasts deficient for caveolin or dynamin, and NIH 3T3 cells knocked down for caveolin expression, was unaffected. Conversely, A-MLV infection of NIH 3T3 and HeLa cells was sensitive to amiloride analogues and actin-depolymerizing drugs that interfere with macropinocytosis. Further manipulation of the actin cytoskeleton through conditional expression of dominant positive or negative mutants of Rac1, PAK1, and RhoG, to increase or decrease macropinocytosis, similarly correlated with an augmented or inhibited infection with A-MLV, respectively. The same experimental perturbations affected the infection of viruses that use clathrin-coated-pit endocytosis or other pathways for entry only mildly or not at all. These data agree with immunofluorescence studies and cryo-immunogold labeling for electron microscopy, which demonstrate the presence of A-MLV in protrusion-rich areas of the cell surface and in cortical fluid phase (dextran)-filled macropinosomes, which also account for up to a half of the cellular uptake of the cell surface-binding lectin concanavalin A. We conclude that A-MLV use macropinocytosis as the predominant entry portal into cells.

IMPORTANCE

Binding and entry of virus particles into mammalian cells are the first steps of infection. Understanding how pathogens and toxins exploit or divert endocytosis pathways has advanced our understanding of membrane trafficking pathways, which benefits development of new therapeutic schemes and methods of drug delivery. We show here that amphotropic murine leukemia virus (A-MLV) pseudotyped with the amphotropic envelope protein (which expands the host range to many mammalian cells) gains entry into host cells by macropinocytosis. Macropinosomes form as large, fluid-filled vacuoles (up to 10 μm) following the collapse of cell surface protrusions and membrane scission. We used drugs or the introduction of mutant proteins that affect the actin cytoskeleton and cell surface dynamics to show that macropinocytosis and A-MLV infection are correlated, and we provide both light- and electron-microscopic evidence to show the localization of A-MLV in macropinosomes. Finally, we specifically exclude some other potential entry portals, including caveolae, previously suggested to internalize A-MLV.

The murine leukemia virus (MLV) belongs to the genus of gamma retroviruses and produce a virion of approximately 90 nm in diameter consisting of a spherical nucleocapsid (the single-strand-RNA [ssRNA] viral genome in complex with viral proteins) surrounded by a lipid bilayer envelope derived from the host cell membrane but studded with viral envelope proteins. The envelope membrane of amphotropic MLV (A-MLV) contains a viral envelope protein (called SU or A-Env), which utilizes the Pit2 sodium-dependent phosphate transporter (solute carrier family 20, member 2 [SLC20A2]) as a cell surface receptor to infect mammalian cells (1, 2). Although initial attachment of virions to the cell surface might be mediated through other factors, including glycosaminglycans (3) or fibronectin (4), Pit2 is required for entry of the virus and infection (1, 2). Pit2 is a conserved membrane protein with five presumed extracellular loops, of which the first loop forms the binding site for A-Env (1). Pit2 is distributed between the cell surface and intracellular stores (5), and upon A-MLV infection, Pit2 is downregulated from the cell surface and localized to an uncharacterized membrane compartment. The known ability of cells to increase their capacity for phosphate influx when deprived of phosphate in the medium may reside not in changes in Pit2 distribution but rather in posttranslational modification of surface-resident Pit2 transporters (6).

Viruses have evolved to utilize practically every known mechanism of endocytosis for cellular entry, including clathrin-coated-pit endocytosis, clathrin-independent internalization pathways, including caveolae and non-caveolin-dependent pathways, and macropinocytosis (7–9). Caveolae are small (50- to 60-nm) omega-shaped invaginations of the plasma membrane carrying a coat structure of caveolin-1 (and -2). They are essentially stable and immobile microdomains on the membrane but have a propensity for internalization when triggered by intracellular signaling and/or virus attachment (7, 10, 11), and some of the factors required for caveola localization and trafficking at the cell surface are becoming elucidated (12, 13). Internalized caveolae communicate with the classical endosomal pathway and the endoplasmic

Received 12 August 2014 **Accepted** 18 November 2014

Accepted manuscript posted online 26 November 2014

Citation Rasmussen I, Vilhardt F. 2015. Macropinocytosis is the entry mechanism of amphotropic murine leukemia virus. J Virol 89:1851–1866. doi:10.1128/JVI.02343-14.

Editor: K. L. Beemon

Address correspondence to Frederik Vilhardt, vilhardt@sund.ku.dk.

doi:10.1128/JVI.02343-14

reticulum (ER)/Golgi apparatus (14, 15). A number of viruses have been proposed to make use of caveolae as entry portal, including the small, nonenveloped virus simian virus 40 (SV40) and BK virus, because their cellular receptors have an affinity for caveolae/lipid rafts (8, 9), which may be enhanced even further by receptor cross-linking by multivalent ligands such as virus particles. However, in some cases, scrutiny reveals that caveolae are not the dominant mode of entry, which becomes clear only in cells devoid of caveolae (16).

Another mode of virus entry is by constitutive or induced macropinocytosis (17–24), which can occur through several distinct mechanisms (lamellipodial and circular ruffles as well as filopodial and blebbing macropinocytosis [8, 24]). All mechanisms rely on small GTPases of the Rho family and actin remodeling to promote formation of cell surface extrusions, which, when falling back onto the cell, entrap a large volume of extracellular fluid to generate a macropinosome from a few hundred nm up to 10 μm in size (8, 24). Physiologically, this process is most pronounced in different types of phagocytes, but other cells in the body can be induced to perform macropinocytosis by growth factors or other forms of stimulation (25). Macropinocytosis is independent of clathrin or other coat proteins, relying instead (according to the specific type of macropinocytosis) on proteins such as phosphoinositol 3-kinase, the small GTPase Rac1 (26) and its effector p21-activated kinase (PAK1) (27, 28), or RhoG (29), which contribute at different time points during the process of macropinosome formation.

It has been claimed that A-MLV binds to cholesterol-enriched microdomains (lipid rafts) on the plasma membrane and is internalized via caveolae (30). However, preliminary morphological observations made by us in the past called us to question this proposition, and we show here with the use of mouse embryonic fibroblasts (MEFs) isolated from caveolin-1 knockout animals and other appropriate cellular models that entry of A-MLV is independent of caveolae and takes place through a macropinocytic pathway.

MATERIALS AND METHODS

Chemicals, antibodies, and cells. Amiloride, *N*-(ethyl-*N*-isopropyl)-amiloride (EIPA), okadaic acid, latrunculin A, and cytochalasin D (Sigma-Aldrich) were prepared in stock solutions in dimethyl sulfoxide (DMSO) and frozen at −80°C. Aliquots were used only a few times before replacement. HeLa cells and NIH 3T3 cells obtained from The Danish Cancer Society were cultured in Dulbecco's modified Eagle medium (DMEM) containing 10% fetal calf serum (FCS) and penicillin-streptomycin. Mouse embryonic fibroblasts (MEFs) generated from wild-type or caveolin-1 knockout mice (31) were obtained from the European Collection of Cell Cultures and cultured in DMEM with 10% FCS, sodium pyruvate, and penicillin-streptomycin. MEFs derived from dynamin-1 knockout mice were obtained from Biotech Research and Innovation Centre (BRIC), and similarly cultured. HeLa cells with conditional expression (tet-off) of dynamin-1-K44A were also obtained from BRIC and were cultured in DMEM containing tetracycline-free 10% FCS and penicillin-streptomycin for 5 days before experimentation. Primary antibodies included rabbit anti-Pit2 antibodies (anti-SLC20A2; Sigma), and rabbit-anti Pit2 antibodies (generously provided by Wayne Anderson, Laboratory of Cellular Oncology, National Cancer Institute, NIH, USA), mouse anti-low-density-lipoprotein receptor (LDL-R) MAb (Santa Cruz Biotechnologies), mouse anti-green fluorescent protein (GFP) MAbs (Roche Biochemicals), rabbit anti-GFP antibodies (Molecular Probes), mouse anti-Myc MAb (9E10; Santa Cruz Biotechnologies), rabbit anti-caveolin-1 antibodies (Cell Transduction Laboratories), mouse anti-lamin A antibodies (Santa Cruz Biotechnologies), mouse anti-human Rac1 MAb (Abcam), mouse anti-RhoA MAb (Upstate Biotechnology), and mouse anti-Cdc42 MAb (Santa Cruz Biotechnologies). All fluorophore-conjugated secondary antibodies, dextrans, cholera toxin B subunit (CTB), concanavalin A (ConA), and phalloidin were from Molecular Probes.

Virus production and cell transduction. In all cases, HEK293T producer cells were Ca_2PO_4 transfected in 10-cm dishes with vector and helper plasmids followed by a medium change the next day. Conditioned medium was collected after 48 h, filtered through a 0.45-μm syringe filter, and then concentrated 20-fold by centrifugation in a Sartorius Vivaspin column.

To produce A-MLV, we used vector plasmids pCNGC expressing GFP or pLacZ in combination with helper plasmids containing wild-type Gag-Pol and the amphotropic envelope protein. For microscopy, we also made use of A-MLV prepared from plasmids encoding a Gag-yellow fluorescent protein (YFP) fusion construct, used together with a myristoylation-deficient version of Gag (to obtain high-titer production of virus) (32). The resulting A-MLV Gag-ΔMyr-YFP virus particles carry the YFP moiety in the nucleocapsid; they are fusion competent and disassemble upon entry into the cytosol (thus diluting the YFP fluorescence). As controls of specificity, MLV was also produced with the ecotropic envelope protein (E-Env). All MLV-related plasmids were most generously provided by Mary Collins, MRC Medical Molecular Virology Centre, University College London, London, United Kingdom. Additionally, we made use of adenovirus 5 (Ad5) expressing GFP (kindly provided by Peter Holst, Department of International Health, Immunology, and Microbiology, Copenhagen University, Copenhagen, Denmark) and lentivectors pseudotyped with vesicular stomatitis virus antigen G (VSV-G).

For conditional expression of Rac1, Cdc42, PAK1, RhoA, or RhoG mutants in NIH 3T3 or HeLa cells, we used helper plasmid 8.91 and lentivector pLOX TW, which express transgenes under a tetracycline (rtTA)-responsive promoter. All constructs have been described previously (33), except for RhoG and RhoG-Q61L (cDNA kindly provided by S. M. Ellerbroek and K. Burridge, Department of Cell and Developmental Biology, Lineberger Comprehensive Cancer Center, University of North Carolina, Chapel Hill, NC, USA), which were PCR amplified with sticky primers and inserted into BamHI/SalI-restricted pLOX TW. For transgene delivery, virus particles were pseudotyped with either E-Env for transduction of NIH 3T3 cells or with VSV-G for transduction of HeLa cells. These virus particles were then used for superinfection of established rtTA-expressing NIH 3T3 or HeLa cell lines previously transduced with pLOX TW rtTA, and tested by saturating superinfection with pLOX TW GFP and flow cytometric analysis to obtain populations with little runoff transcription and high levels of induction. For infection assays, cells were induced overnight with 0.1 μg/ml doxycycline before virus challenge, and doxycycline was maintained until virus was washed away after incubation. Transgene expression ranged between 70 and 90% for the different constructs in NIH 3T3 and HeLa cells, being higher in the latter cell type, as determined by immunofluorescence. Expression of Rac1-N17A was difficult to maintain in the populations (about 60 to 70% transduced cells), perhaps because of negative selection during culture in response to low levels of runoff transcription from this vector. For stable knockdown of caveolin-1, we made use of the E-Env-pseudotyped short-hairpin RNA (shRNA) lentivector pGIPZ Cav1 9666 and a nonsilencing control (target sequence for caveolin silencing, TATAGTCTCCAATTGATG; control nonsilencing sequence, ATCTCGCTTGGGCGAGAGTAAG; Open Biosystems) which coexpresses GFP as a marker to transduce NIH 3T3 cells. GFP-expressing cells were enriched further to above 85% purity by flow-assisted cell sorting on a Becton Dickinson Aria flow cytometer for experimentation.

Infection assays. NIH 3T3 cells, HeLa cells, or MEFs in 48-well culture dishes were infected with MLV expressing GFP and pseudotyped with amphotropic or ecotropic envelope proteins, Ad5 expressing GFP, or lentivectors expressing GFP and pseudotyped with VSV-G. Most assays were

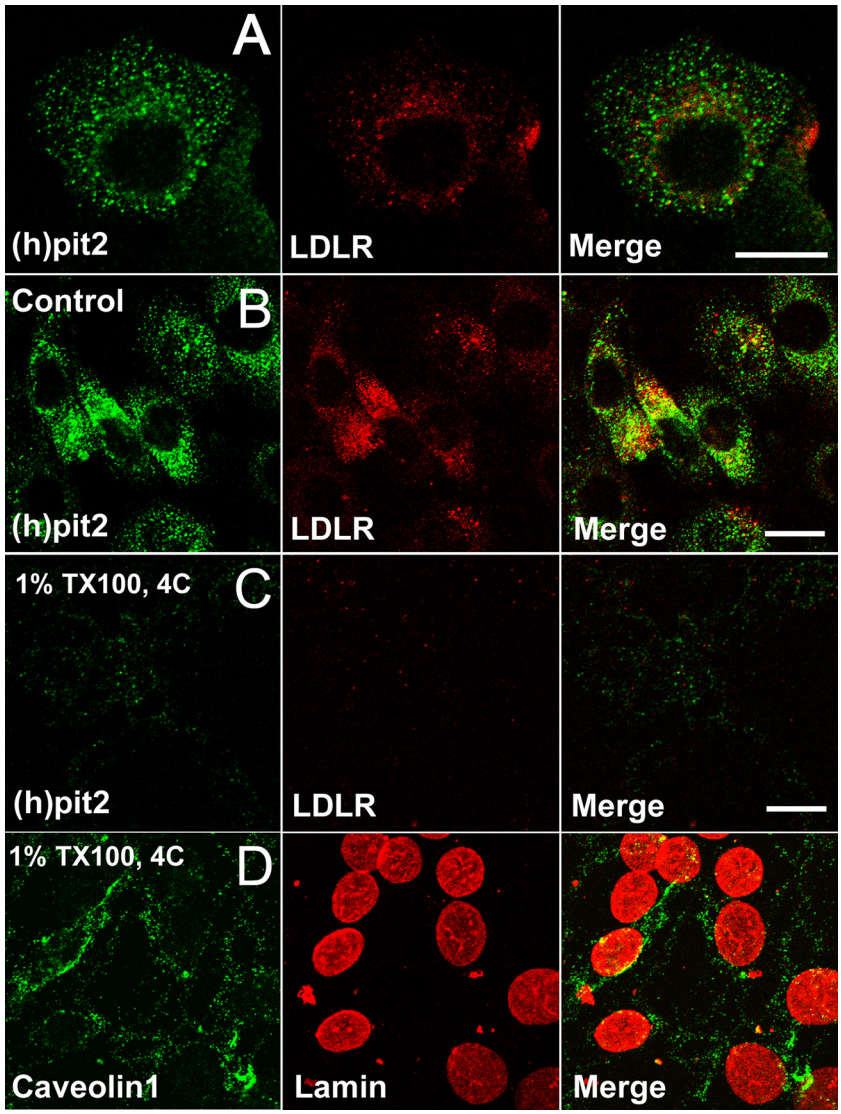

FIG 1 Pit2 is predominantly soluble in ice-cold TX-100. (A) NIH 3T3 cells overexpressing human Pit2 were fixed and stained with anti-LDL-R MAb and polyclonal rabbit anti-Pit2 antibodies followed by secondary fluorophore-conjugated antibodies. Pit2 can be localized in vesicular profiles scattered in the cytoplasm but concentrated around the nucleus, where LDL-R also resides in the recycling endosome compartment. (B to D) NIH 3T3 cells were treated for 15 min without agitation on ice without (control) or with 1% TX-100 before fixation and processing for immunofluorescence as described in Materials and Methods to visualize Pit2, LDL receptor, caveolin-1, or lamin A. Note that the majority of both LDL receptor and Pit2 is extracted by TX-100 (C), while caveolin-1 and lamin A are not (D). Bars, 10 μm.

carried out with duplicate wells. Unless otherwise specified, no Polybrene was added during virus incubations. Cells were incubated either for 2 h or overnight with virus, as specified, concurrent with drug treatment or transgene induction, before two 1-min washes in 40 mM calcium citrate, 10 mM KCl, 135 mM NaCl (pH 3.0) at room temperature to dissociate surface-bound virus particles. The cells were washed in medium and returned to 24 h of further culture before analysis of GFP expression by flow cytometry on a Becton Dickinson Accuri C6 flow cytometer. In all instances, we chose drug concentrations so that only minimal toxicity with no cell death (visual inspection) was achieved. The titers of A-MLV determined on the different cell types used in this study were $6.9 \times 10^5 \pm 0.3 \times 10^5$ for wild-type (wt) MEFs, $1.1 \times 10^6 \pm 0.1 \times 10^6$ for NIH 3T3 cells, and $2.6 \times 10^6 \pm 0.9 \times 10^5$ for HeLa cells (means and standard errors of the means [SEM]; $n \geq 6$). For suspension-mediated caveola internalization in HeLa cells, A-MLV containing Gag-YFP together with Alexa 647-conjugated ConA (2.5 μg/ml) was bound to attached HeLa cells at 4°C for 1 h in the presence of Polybrene (8 μg/ml) before cells were dislodged into cold phosphate-buffered saline (PBS) by pipetting and scraping. Cells were transferred to Eppendorf tubes and then incubated for 15 min with rotation at 4°C or 37°C before being washed. Cells were then centrifuged onto microscope slides (1,500 × *g*, 2 min, 4°C) and processed for immunofluorescence to visualize caveolin-1 in relation to Gag-YFP and ConA-Alexa 647.

Morphological analysis. Immunofluorescence was performed essentially as described previously (34). Briefly, cells cultured in 8-chamber slides were fixed in 2% paraformaldehyde in phosphate buffer, pH 7.2, for a minimum of 30 min followed by rinsing in PBS. Blocking and antibody buffer consisted of PBS with 5% normal goat serum and 0.2% saponin, and primary antibodies were detected by Alexa-conjugated secondary goat-anti mouse or rabbit IgG antibodies (Molecular Probes), sometimes with Alexa 633-conjugated phalloidin to reveal cell shape.

To visualize A-MLV internalization HeLa cells expressing Rac1-V12G were incubated at 4°C with A-MLV virions containing Gag-YFP

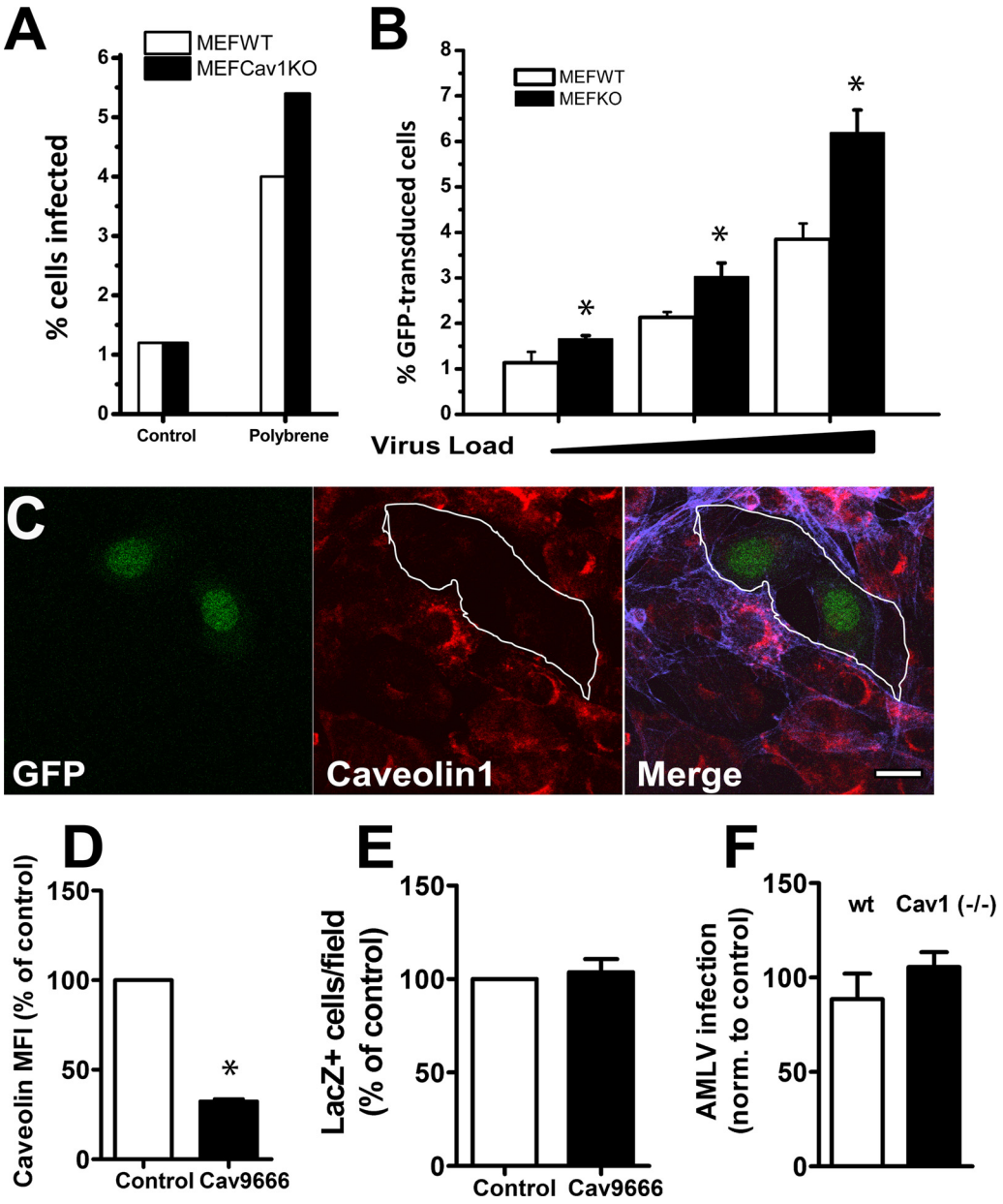

FIG 2 Infection of MEF or NIH 3T3 cells by A-MLV does not require caveolae and is pH independent. (A and B) MEFs derived from wild-type or caveolin-1 knockout mice (KO) were challenged with GFP-expressing A-MLV in the absence or presence of 8 μg/ml Polybrene overnight and then incubated for a further 24 h before flow-cytometric analysis of GFP-expressing cells. Results are the percent GFP-positive cells in the total viable cell population. Panel A shows representative results from a single experiment, while panel B shows means and SEM from three individual experiments with Polybrene added. (C) NIH 3T3 cells coexpressing caveolin-1 shRNA (cav9666) and GFP as a marker were processed for immunofluorescence using anti-caveolin-1 MAb and Alexa 633-conjugated phalloidin. Cells expressing caveolin-1 shRNA (outlined), identified by concurrent GFP expression, were depleted of caveolin-1 protein. Bar, 10 μm. (D) Knockdown of caveolin-1 in NIH 3T3 cells expressing control shRNA or caveolin-1 shRNA was assessed by flow cytometry of the GFP^+ gated population using anti-caveolin MAb followed by goat anti-mouse Alexa 633-conjugated antibodies. Results are expressed as normalized fluorescence intensity (MFI) (mean and SEM) of caveolin staining from three independent experiments. (E) NIH 3T3 cell populations transduced with control or caveolin shRNA-expressing vectors were FACS enriched for GFP expression (>85%) and then challenged overnight with A-MLV expressing the LacZ gene as the reporter gene. After 24 h of further incubation, cultures were processed for X-Gal cytochemistry, and blue cells were counted. The graph shows the number of blue cells per field normalized to cells expressing control shRNA (means and SEM; $n = 3$). (F) Wt and $Cav1^{-/-}$ MEFs were preincubated with 50 mM ammonium chloride and then challenged with GFP-expressing A-MLV for 1 h before an acid wash. Cells were cultured for a further 24 h before flow-cytometric analysis of GFP expression. Results are levels of A-MLV infection normalized to values for untreated control cells (means and SEM; $n = 3$). *, significantly different from the control.

and either Alexa 633-conjugated cholera toxin B subunit (CTB) or concanavalin A. After being washed, cells were chased at 37°C together with 250 μg/ml tetramethyl rhodamine (TMR)-conjugated dextran (70,000 kDa) for 15 to 60 min followed by a washing before live imaging of cells for up to 15 min at room temperature. Imaging of live cells or fixed slides was performed with a Zeiss LSM510 confocal laser scanning microscope with a C-Apochromat X63, NA 1.2 oil immersion objective, using the argon 488 nm, and helium-neon 543- and 594-nm

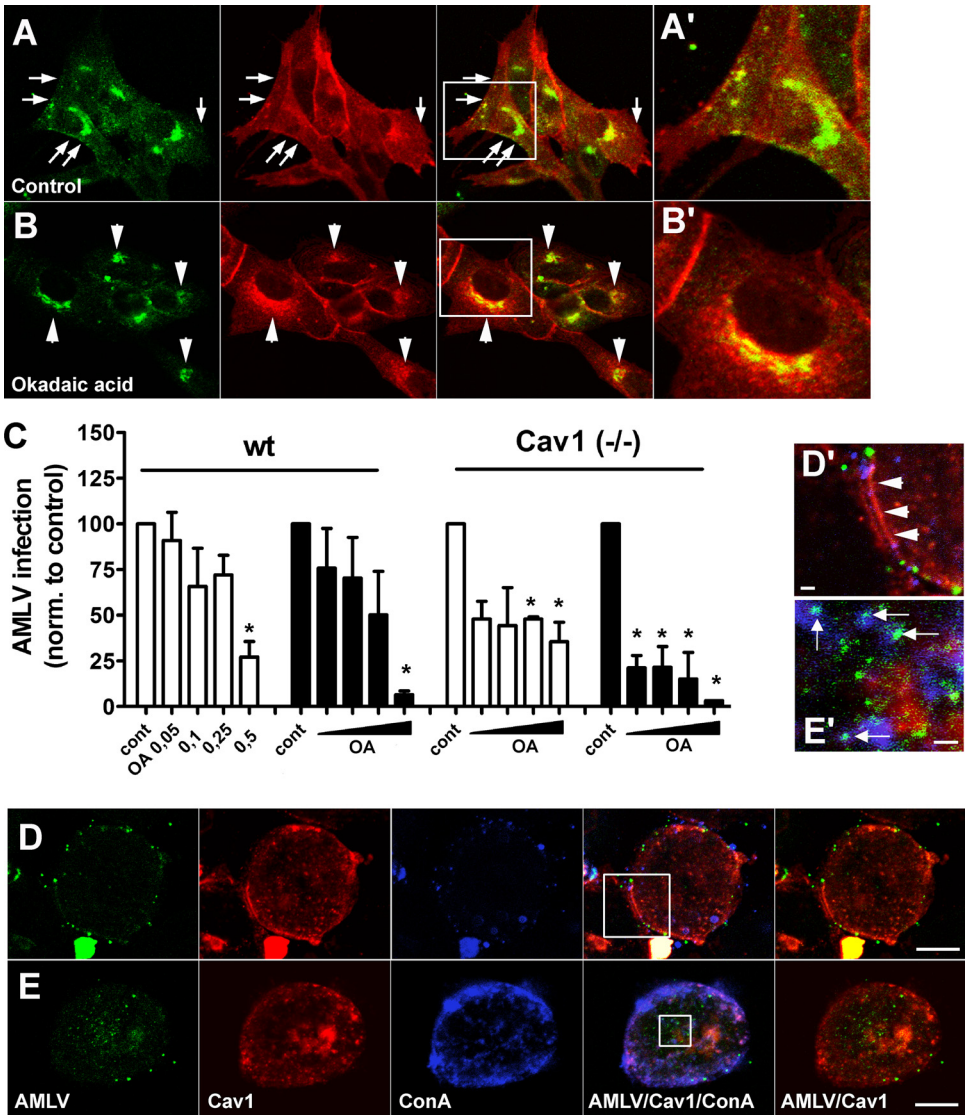

FIG 3 Effect of stimulated caveolae internalization on A-MLV uptake and infection. (A and B) Wt MEFs were treated with vehicle (control) or 0.1 μM okadaic acid for 30 min in the presence of Alexa 647-conjugated CTB (pseudocolored red) before processing for immunofluorescence with anti-caveolin-1 antibody (green). Note that surface-localized caveolin and caveolae (B, arrows) disappear upon okadaic acid treatment, and perinuclear accumulation of CTB is increased (A, arrowheads). (A′ and B′) Boxed areas in panels A and B at a higher magnification. Bars, 10 μm. (C) Wt and caveolin-1-null MEFs were treated with vehicle or increasing concentrations (μM) of okadaic acid (OA) as indicated, either as a 30-min preincubation (white bars) or added simultaneously with A-MLV (black bars). Cells were incubated with A-MLV expressing GFP for 1 h and were then acid washed and returned to culture overnight before flow-cytometric analysis of GFP-expressing cells. Results are expressed as levels of A-MLV infection normalized to those of untreated control cells (means and SEM; $n = 3$). *, significantly different from the control. (D and E) HeLa cells were incubated with A-MLV-GAG-YFP together with 2.5 μg/ml Alexa 647-conjugated ConA in the cold, washed, and then brought into suspension and incubated for 15 min at 4°C or 37°C, before cells were spun down onto slides at 4°C. Immunofluorescence was then performed to visualize caveolin-1 distribution (red) in relation to A-MLV and ConA. Note that surface-localized caveolin-1/caveolae in cells kept at 4°C (D′, arrowheads) are internalized upon incubation at 37°C but that internalized A-MLV–Gag-YFP preferentially colocalizes with internalized ConA (E′, arrows) or is present in unlabeled structures. (D′ and E′) Boxed areas in panels D and E at a higher magnification. Bars, 10 μm (D and E) and 1 μm (D′ and E′). Images are representative of two independent experiments.

laser lines for excitation of Alexa 488 and of Alexa 568 and 633, respectively. Optical sections (1.0 to 1.5 μm) were collected and saved as 1,024- by 1,024-pixel images at an 8-bit resolution before import into Adobe Photoshop for compilation.

To gauge the Triton X-100 (TX-100) solubility of Pit-2, 3T3 cells transfected with human Pit2 were cultured in 8-chamber slides and extracted in 0.5 to 1% TX-100 in Hanks balanced salt solution (HBSS) for 15 min on ice before gentle aspiration and fixation for immunofluorescence with rabbit anti-pit2 and rabbit anti-caveolin polyclonal antibodies, together with mouse anti-LDL-R or anti-lamin A MAbs as described above.

For cryo-immunogold labeling, mouse (*Mus dunni*) fibroblasts were challenged with Gag-YFP-containing A-MLV particles for 4 h before fixation in 2% paraformaldehyde (PFA) and 0.1% glutaraldehyde in phosphate buffer (pH 7.2) (a kind contribution from L. Pedersen, Department of Molecular Biology and Genetics, Molecular Cell and Developmental Biology, Aarhus University, Aarhus, Denmark). Subsequent gelatin embedding, ultracryosectioning, and cryo-immunogold labeling were per-

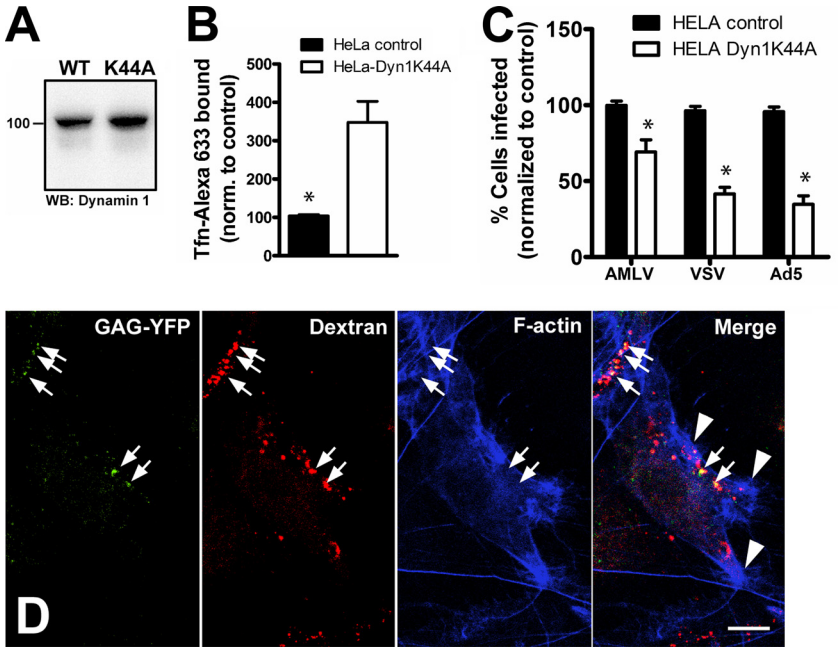

FIG 4 A-MLV uptake and infection does not require dynamin. (A) Cell lysates of control or HeLa cells expressing dominant negative dynamin-1-K44A were Western blotted with mouse anti-dynamin-1 MAb. WT, wild type; WB, Western blot. (B) Cell surface binding of Alexa 633-conjugated transferrin (Tfn-Alexa 633) in control or dynamin-1-K44A-expressing cells was determined by flow cytometry. (C) HeLa control or dynamin-1-K44A-expressing cells were challenged with A-MLV, VSV-G-pseudotyped lentivector, or Ad5, all expressing GFP. Results are percent GFP-positive cells normalized to control cells (means and SEM from three independent experiments). *, significantly different from the control. (D) Dynamin-1-null MEFs were incubated with A-MLV, containing Gag-YFP for visualization, together with TMR-conjugated dextran as a fluid phase tracer of endocytosis for 30 min before processing for immunofluorescence with Alexa 647-conjugated phalloidin to visualize F-actin. Note that virus particles can be seen in large fluid-filled endocytic compartments (arrows), often near areas of F-actin ruffling (arrowheads). Bar, 10 μm.

formed as described previously (34) with anti-GFP MAb followed by treatment with secondary 10-nm-gold-conjugated goat-anti mouse antibodies. Sections were examined in a Philips CM100(a) TWIN electron microscope (Philips, Eindhoven, The Netherlands).

Statistical analysis. Data were analyzed with Student's *t* test, and significance levels were defined as *P* values less than 0.05.

RESULTS

The Pit-2 receptor is predominantly TX-100 soluble, and A-MLV infection does not require caveolae. It has been reported that A-MLV is internalized through caveolae, and correspondingly that the A-Env cell surface receptor Pit2 is a lipid raft-associated protein (30). Proteins contained in caveolae and lipid rafts are insoluble in cold nonionic detergents such as TX-100, and therefore we first investigated the sensitivity of Pit-2 in NIH 3T3 cells on ice to extraction with 1% TX-100. By immunofluorescence, overexpressed human Pit-2 was mainly intracellularly and partially colocalized with the recycling receptor LDL-R in perinuclear endosomes (Fig. 1A and B). Extraction of cells with TX-100 greatly reduced immunoreactivity for both Pit-2 and the nonraft protein LDL-R (compare Fig. 1B with C), whereas, as expected, it failed to remove either caveolin-1 itself or the insoluble intermediary filament lamin A (Fig. 1D). We therefore conclude that Pit-2 in the absence of ligation predominantly resides outside lipid rafts. Caveolin-1 is essential for the formation of caveolae (35), and to specifically address the role of caveolae in A-MLV infection (30), we made use of murine embryonic fibroblasts (MEFs) from characterized caveolin-1 knockout mice (31) as target cells. A-MLV expressing GFP was incubated with MEFs overnight with or without Polybrene (a polycation which increases virus binding to the cell surface) and incubated for a further 24 h before flow-cytometric analysis of GFP expression. As seen in Fig. 2A and B, the absence of caveolae did not inhibit A-MLV infection, and in the presence of Polybrene, infection was even moderately increased in caveolin-null MEFs. To exclude potential cell type-specific effects, we knocked down caveolin-1 expression in NIH 3T3 cells, also used in the original study (30), by transduction with caveolin-1 shRNA retroviral particles pseudotyped with E-Env (Fig. 2C to E). Following a cell sorting step by FACS to enrich the population expressing the shRNA construct (gating of GFP coexpression to ca. 85% purity), NIH 3T3 cells were then challenged with A-MLV expressing the LacZ gene as a reporter gene overnight and after 24 h of culture subsequently processed for X-Gal (5-bromo-4-chloro-3-indolyl-β-D-galactopyranoside) staining of infected cells. Despite a 70% reduction in caveolin expression by Cav1-9666 shRNA, infection of A-MLV was not affected in NIH 3T3 cells (Fig. 2E). We also tested the pH dependence of A-MLV infection by alkalizing the endosomal compartment with ammonium chloride. We find that A-MLV infection in neither MEFs (Fig. 2F) nor NIH 3T3 cells (data not shown) is affected by endosomal alkalization as performed in the original study (30).

A-MLV uptake and infection does not correlate with stimulated internalization of caveolae. To exclude the possibility that A-MLV in the absence of caveolae changed its normal uptake route to other portals of entry, we also performed experiments to separate caveolae from A-MLV internalization and infection. In the original study (30), the drug okadaic acid was used to induce

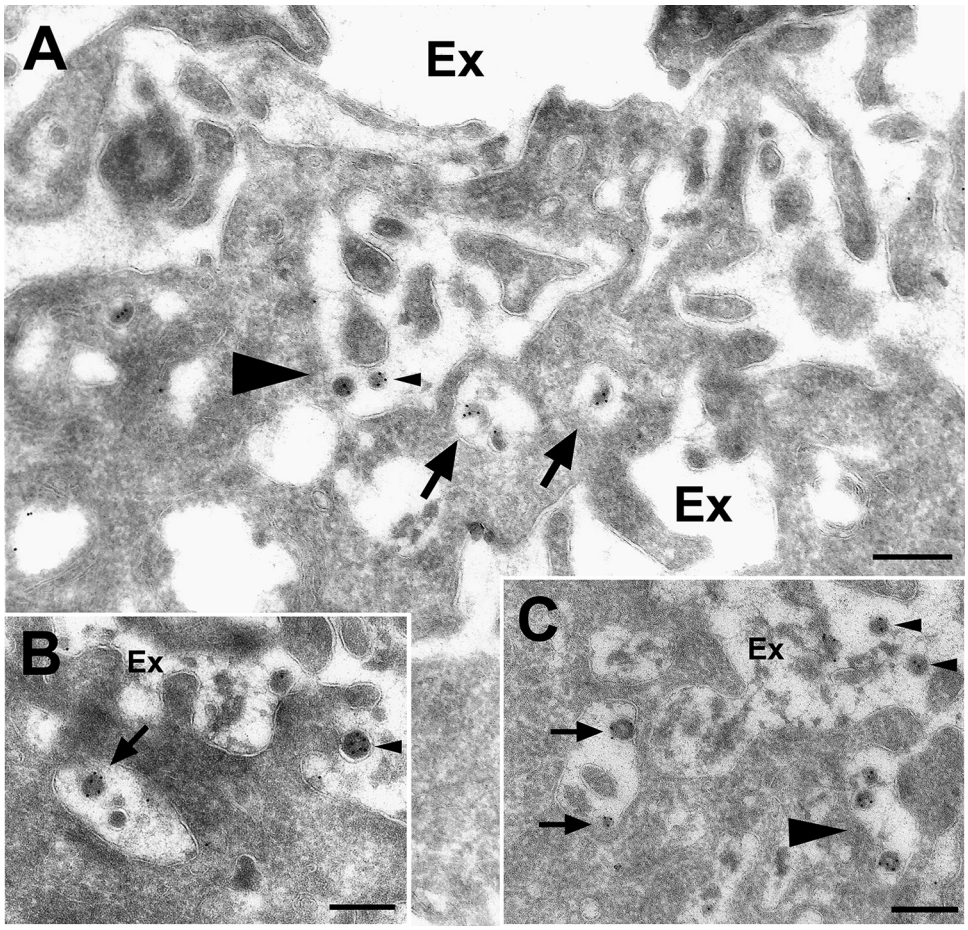

FIG 5 A-MLV particles are present in areas of cell surface ruffling and macropinosome profiles. *M. dunni* tail fibroblasts were incubated with A-MLV particles containing Gag-YFP for 4 h before washing, fixation, and processing for cryo-immunogold labeling with rabbit anti-GFP antibodies. (A to C) On the plasma membrane, A-MLV particles (small arrowheads) were localized in cell surface areas with extensive membrane ruffling and formation of enclosed volumes that could potentially proceed to macropinosome formation (A and C, large arrowheads). Inside the cells, virus particles could be identified in large surface-proximal vacuoles (small arrows) devoid of cellular surface processes indicative of macropinosomes. Ex, extracellular space. Bars, 250 nm.

internalization of caveolae to either block (drug preincubation) or promote (concurrent drug and virus incubation) A-MLV internalization. Okadaic acid is an inhibitor of protein Ser/Thr phosphatases PP1 and PP2A and is known to cause internalization of caveolae and their aggregation into larger unphysiological structures (36) in addition to many other effects. First, we verified in MEFs that 30 min of okadaic acid treatment caused the disappearance of caveolae from the cell surface (Fig. 3A and B). This was paralleled by an increased internalization and perinuclear accumulation of CTB, which in part is internalized by caveolae (37). Then, wt and caveolin-1-null MEFs were incubated with okadaic acid starting either 30 min before or concurrent with a 1-h challenge with A-MLV. As seen in Fig. 3C, okadaic acid, irrespective of pretreatment, caused a dose-dependent decrease in A-MLV infection, and importantly, this inhibitory effect was present in both wt and caveolin-deficient cells and therefore independent of caveolae. We sought to obtain a more physiological correlate of caveola internalization and made use of the fact that bringing adherent cells into suspension causes the internalization of caveolae and lipid rafts (38). We used HeLa cells for this purpose because of their higher infection rate with A-MLV. Adherent cells were exposed to A-MLV virions with Gag-YFP incorporated into the nucleocapsid (32) for visualization and then brought into suspension at 4°C. In addition, we used fluorophore-conjugated versions of the lectin concanavalin A (ConA), which binds terminal α-D-mannosyl and α-D-glucosyl groups in glycoproteins and glycolipids as a general marker of the cell surface. After a washing, cells were retained at 4°C or shifted to 37°C under rotation for 15 min before being gently centrifuged onto microscopic slides and fixed. Cells were stained with anti-caveolin-1 antibodies, and medial confocal planes of the cells were obtained in the microscope. Figure 3D and E show that caveolae are present on the surfaces of cells suspended and retained at 4°C, while cells suspended at 37°C showed accumulation of caveolin-1 staining in intracellular structures. Notably, despite internalization of caveolae, the majority of internalized A-MLV, identified by Gag-YFP expression, localized with ConA-labeled structures or structures of unknown identity (no label). We conclude that A-MLV infection does not require and is independent of caveolae.

Uptake and infection of A-MLV is independent of dynamin. Clathrin-coated pits share with caveolae and RhoA-regulated clathrin- and caveolin-independent carriers the requirement for dynamin function to pinch off the budding vesicles from the plasma membrane (7, 39, 40). We therefore tested the effect of

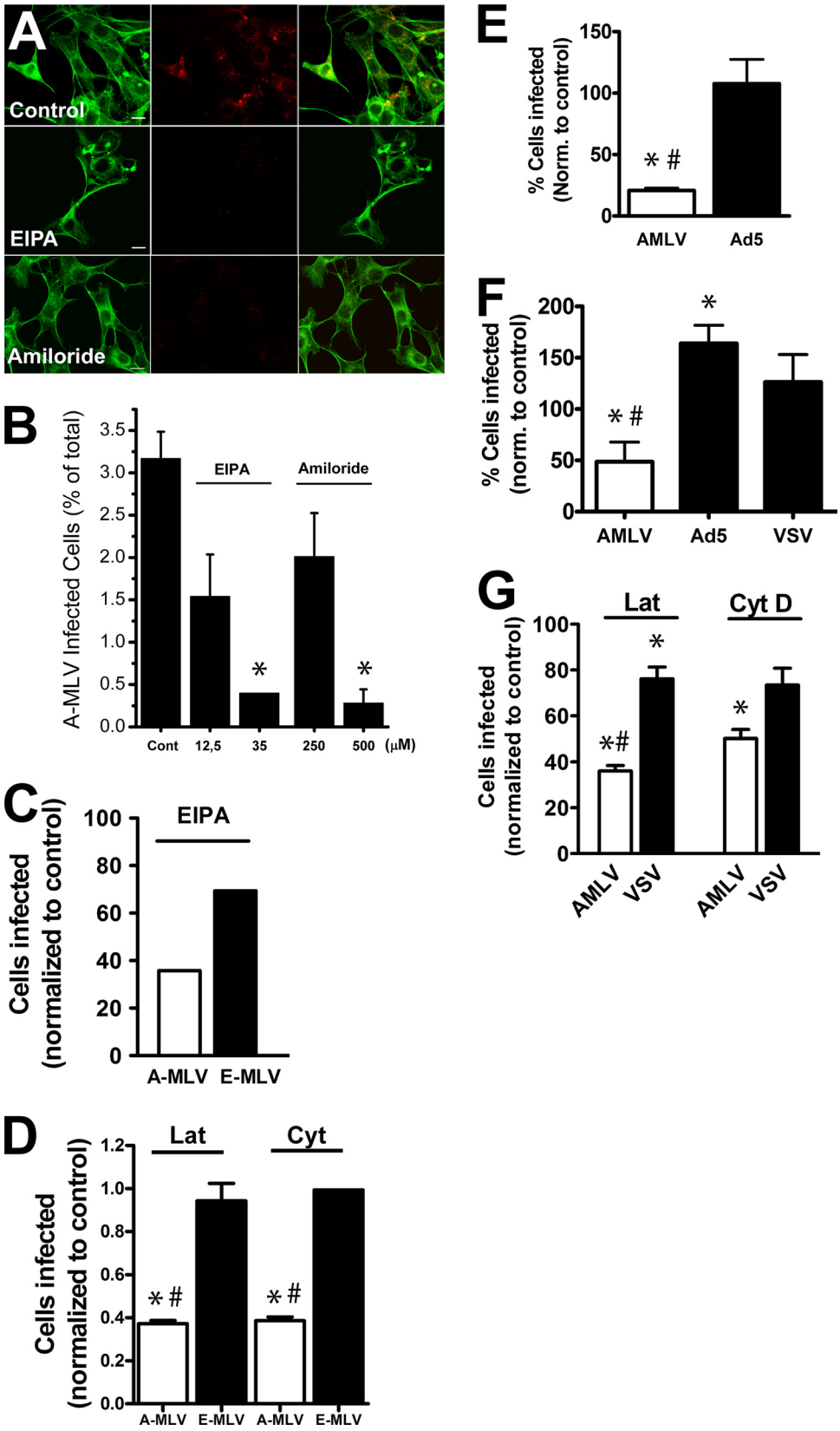

FIG 6 A-MLV infection is specifically affected by drugs that inhibit macropinocytosis. (A) NIH 3T3 cells were incubated with TMR-conjugated dextran (70 kDa; red) at a concentration of 250 μg/ml with or without 50 μM EIPA or 500 μM amiloride for 1 h before fixation and visualization using Alexa 488-conjugated phalloidin (green) as a counterstain. Bars, 10 μm. (B) NIH 3T3 cells were treated with EIPA or amiloride at the indicated concentrations concurrent with A-MLV incubation overnight and then analyzed for GFP expression by flow cytometry 24 h later. Data are percent GFP-expressing cells (mean and SEM compiled from

conditional expression (tet-off) of dominant negative dynamin-1-K44A in HeLa cells. Expression and function of dynamin-1-K44A was first confirmed by Western blotting and surface binding of Alexa 633-conjugated transferrin, which increased more than 3-fold due to trapping of transferrin receptor, a classical clathrin-coated-pit receptor, on the surface (Fig. 4A and B). Control cells and cells expressing dynamin-1-K44A were then challenged with GFP-expressing A-MLV. To address specificity, we also infected cells with lentivector pseudotyped with vesicular stomatitis virus G antigen (VSV-G) and adenovirus 5 (Ad5), which are both internalized through clathrin-coated pits by different known receptors (41, 42). As shown in Fig. 4C, dynamin-1-K44A expression caused a moderate (30%) drop in A-MLV infection but markedly inhibited lentivector and Ad5 infection, by 60% and 65%, respectively. Finally, in MEF dynamin-1-negative cells we examined uptake of A-MLV particles containing a Gag-YFP fusion construct for visualization. Cells were incubated with A-MLV–Gag-YFP in the cold, washed, and then chased with tetramethylrhodamine (TMR)-conjugated dextran as a fluid-phase marker for half an hour before fixation and phalloidin staining to reveal F-actin and cell shape. Internalized Gag-YFP-labeled particles could be observed in surface-proximal vesicles and vacuoles, which were often quite large and often near areas with intense cell surface ruffling, as indicated by F-actin staining (Fig. 4D). We conclude that A-MLV uptake and infection can take place without dynamin function.

Ultrastructural analysis shows A-MLV associated with ruffles and vacuoles. Our morphological observations above indicated that A-MLV particles were associated with ruffled surface areas and large endocytic elements. We therefore subjected mouse (*M. dunni*) tail fibroblasts, which are readily infected by A-MLV, to ultrastructural analysis by cryo-immunogold labeling after 4 h of incubation with A-MLV containing Gag-YFP. Figure 5A and C (arrowheads) show attachment of A-MLV particles to highly ruffled areas of the plasma membrane and in convoluting and invaginating profiles of the cell surface. Inside the cells, virus particles localized to large vacuolar elements, macropinosomes, near the cell surface (Fig. 5A to C, arrows), although in the absence of cell surface staining, we cannot rule out the possibility that some of these profiles are connected with the cell surface. We did not observe virus particles in caveolae or clathrin-coated pits (data not shown).

Drugs that inhibit macropinocytosis also block A-MLV infection. These observations suggested to us that A-MLV gained entry into host cells through macropinocytosis, similar to a number of other pathogens of both bacterial and viral origin (8). Amiloride, a clinical inhibitor of the Na^+/H^+ exchanger situated in the plasma membrane, and its analogue *N*-(ethyl-*N*-isopropyl)-amiloride (EIPA) are commonly used inhibitors of macropinocytosis (26). First, we tested the proficiency of amiloride treatment to block macropinocytosis in NIH 3T3 cells allowed to take up fluorophore-conjugated 70-kDa dextran. This probe is too large to undergo pinocytosis and is a commonly used marker of macropinocytosis. As seen in Fig. 6A, both amiloride and EIPA inhibited the uptake of dextran in NIH 3T3 cells. We then tested the effect on A-MLV infection. Figure 6B shows that both EIPA and amiloride inhibited infection with A-MLV in a dose-dependent fashion. The inhibitory effect of EIPA noted above was specific for A-MLV, as infection of MLV pseudotyped with the ecotropic envelope protein (E-MLV), which utilizes trafficking of cationic amino acid transporter 1 (CAT-1) through an unknown clathrin-independent pathway for entry (43), was affected to a much smaller extent (Fig. 6C). To expand our observations to cell types other than murine fibroblasts, we also studied effects in HeLa cells. As seen in Fig. 6E and F, A-MLV infection in HeLa cells was also susceptible to EIPA and amiloride inhibition, and again the effect was specific for A-MLV, as adenovirus 5 (Ad5)- and VSV-pseudotyped lentivectors, which are both internalized through clathrin-coated pits, were not inhibited. In fact, A-MLV infection was moderately increased by amiloride (Fig. 6F). Macropinocytosis also depends on actin dynamics. We therefore also compared the effect of F-actin depolymerization with low concentrations of either latrunculin A (200 nM) or cytochalasin D (250 μM) on infectivity of A-MLV or control virus in NIH 3T3 cells and HeLa cells. As shown in Fig. 6D and G, both drugs decreased A-MLV infection by roughly 60%, while E-MLV infection in NIH 3T3 cells was only marginally decreased, and infection with VSV-pseudotyped lentivectors decreased only by ca. 20% in HeLa cells.

F-actin and small GTPases are required for A-MLV infection. Amiloride and EIPA work through inhibition of the Na^+/H^+ exchanger, which provides a slightly alkaline submembranous pH essential for Rac1 and Cdc42 localization to the membrane (26). These small GTPases, in particular Rac1, are required to orchestrate the actin rearrangement necessary for membrane ruffling and macropinocytosis to occur (8, 27, 44). One of the downstream targets of Rac1 is p21-activated kinase 1 (PAK1), which is required at several steps of macropinocytosis, including closure of macropinocytic vacuoles formed from lamellipodial ruffles (24, 28). We therefore tested the effect of conditional (doxycycline-inducible) expression of dominant negative Rac1-N17A or PAK1-K299A or dominant positive Rac1-V12G mutants on A-MLV infection in NIH 3T3 cells. We also included expression of the irrelevant protein β-synuclein (βSNC) as a vector control of transduction and additionally dominant negative RhoA-N19A as

three independent experiments). (C) NIH 3T3 cells were incubated with 35 μM EIPA concurrent with overnight challenge with MLV pseudotyped with either A-Env (A-MLV) or E-Env (E-MLV) and analyzed by flow cytometry. Results are the percent GFP-positive cells, normalized to controls, and are representative of two independent experiments. (D) NIH 3T3 cells were treated with 200 nM latrunculin A (Lat) or 250 μM cytochalasin D (Cyt) concurrent with E-MLV or A-MLV challenge overnight and analyzed as described above. Results are expressed as the percent GFP-positive cells, normalized to controls (infection without drugs), and are means and SEM from three independent experiments. (E) HeLa cells were incubated with GFP-expressing A-MLV or adenovirus 5 (Ad5) in the presence of 50 μM EIPA for 2 h, acid washed, and then incubated overnight before flow-cytometric analysis of GFP-positive cells. Results are the percent infected cells, normalized to values for untreated control cells (mean and SEM; $n = 3$). (F) HeLa cells were challenged with GFP-expressing A-MLV, Ad5, or VSV-pseudotyped lentivector for 2 h in the presence of 500 μM amiloride and treated as described above. Results are means and SEM ($n = 3$) and were normalized to values for untreated control cells. (G) HeLa cells were challenged overnight with GFP-expressing A-MLV or VSV-pseudotyped lentivector in the presence of latrunculin (200 nM) or 250 μM cytochalasin D as indicated. Data are the percent GFP-positive cells normalized to controls (means and SEM from three independent experiments). *, significantly different from the control. In panels D to F, the pound sign indicates that the effect of drug treatment was significantly different at a P value of <0.05 between A-MLV and control virus.

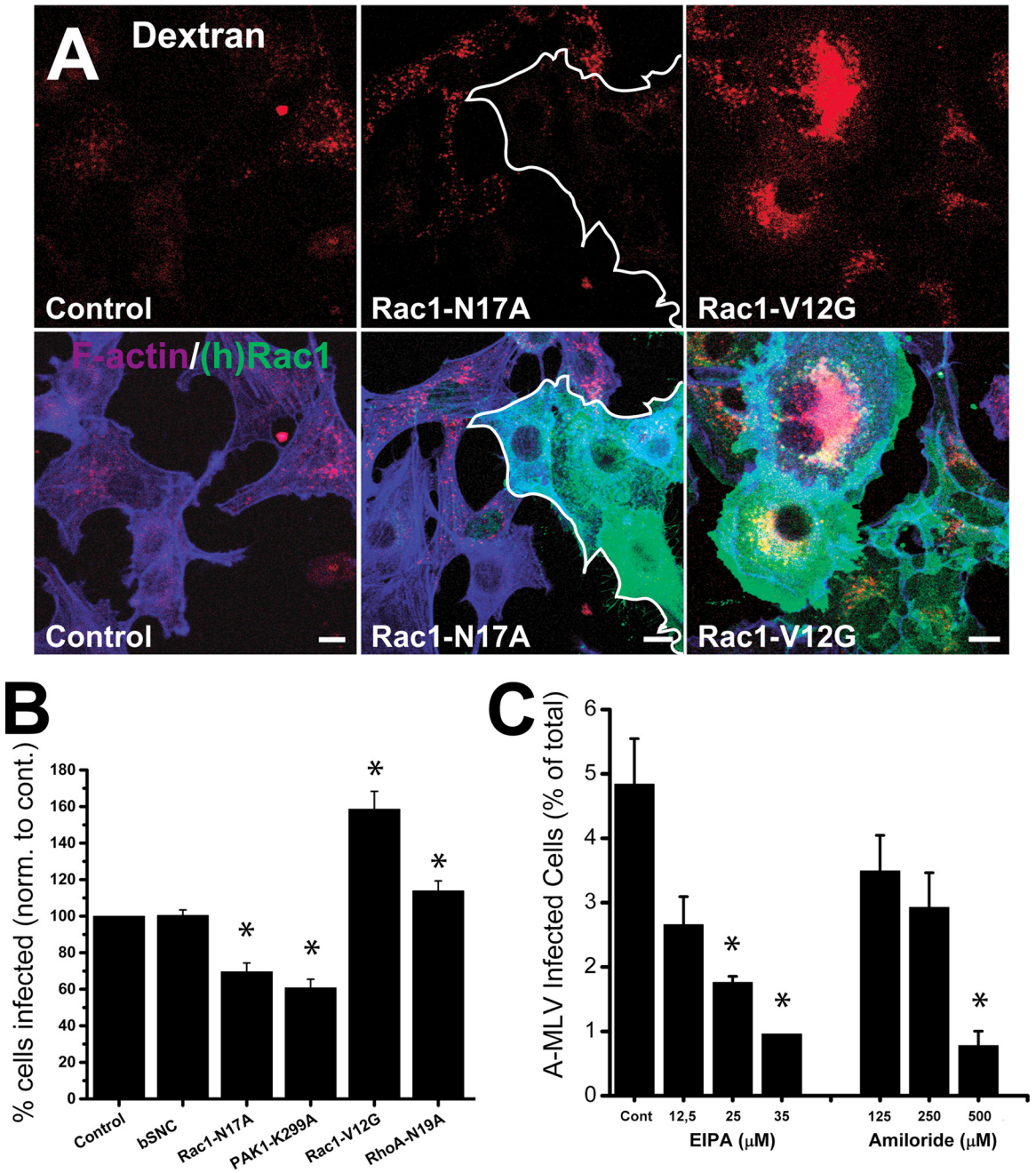

FIG 7 A-MLV infection in NIH 3T3 cells can be modulated by expressing F-actin regulatory proteins involved in macropinocytosis. (A) NIH 3T3 cells transduced with Rac1-N17A, Rac1-V12G, or (as a control) only the rtTA protein were incubated with 70-kDa TMR-conjugated dextran (red) for 1 h and then processed for immunofluorescence to visualize transgene expression (mouse anti-myc MAb; green) and effect on F-actin (Alexa 647-conjugated phalloidin; blue). Note that expression of Rac1-N17A (cells outlined in white) diminishes uptake of dextran, while Rac1-V12G causes cell flattening with lamellipodium extension, surface ruffling, and increased uptake of dextran. Bars, 10 μm. (B) NIH 3T3 cell lines conditionally expressing either β-synuclein (additional control) or Rac1 or PAK1 mutant transgenes as indicated were incubated with A-MLV overnight and analyzed by flow cytometry for GFP expression. Results are the percent GFP-positive cells normalized to values for rtTA control cells (mean and SEM; $n = 3$). (C) NIH 3T3 cells expressing Rac1-V12G were incubated with A-MLV in the presence of EIPA or amiloride at the indicated concentrations overnight and analyzed by cytometry as described above. The results are absolute percentages of GFP-positive cells (means and SEM from three independent experiments). *, significantly different from the control.

a form of control for small GTPase specificity, as RhoA is not known to be associated with macropinocytic processes (but, as noted above, it regulates a clathrin- and caveolin-independent endocytosis pathway). Transduction efficiency of NIH 3T3 cells following a single round of infection using E-Env pseudotyped lentivectors ranged from 60 to 80% (see Materials and Methods), and care was taken to maintain this level of expression for experiments.

First, we analyzed the cell lines for altered macropinocytic activity by 70-kDa dextran uptake. Shown in Fig. 7A are Rac1-N17A

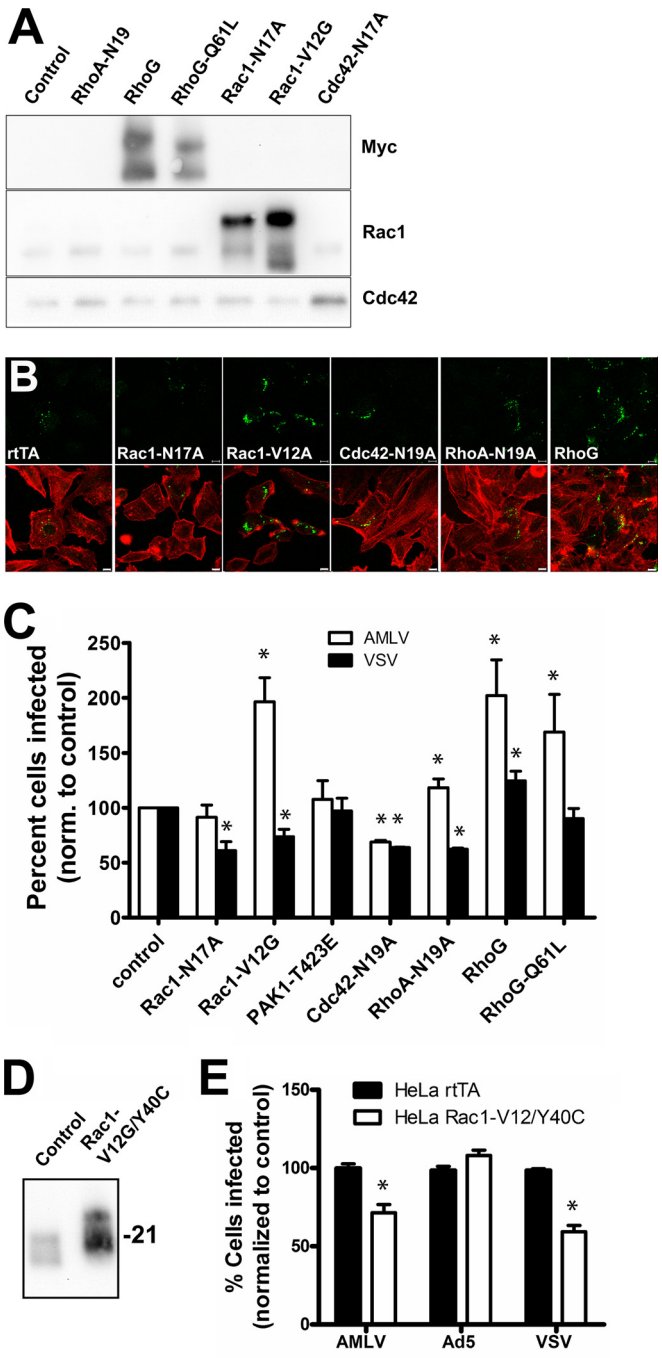

FIG 8 A-MLV infection in HeLa cells is regulated differentially by small GTPases that control endocytosis and actin dynamics. (A) HeLa cells expressing rtTA (control) were transduced with lentivectors for conditional expression of mutant transgenes as indicated and then analyzed by Western blotting after 24 h of doxycycline induction using anti-myc MAb, anti-Rac1 MAb, and anti-Cdc42 MAb. (B) HeLa cells expressing transgenes as indicated were allowed to internalize Oregon green 418-conjugated 70-kDa dextran (green) for 1 h before fixation and staining with Alexa 647-conjugated phalloidin (pseudocolored red) to reveal F-actin. Bars, 10 μm. (C) HeLa cells expressing Rac1, PAK1, Cdc42, RhoA, or RhoG mutants were incubated with GFP-expressing A-MLV or VSV-pseudotyped lentivector overnight, washed, cultured for a further 24 h, and then analyzed by flow cytometry for GFP^+ cells. The data are the percent infected cells normalized to values for control (rtTA) cells (means and SEM; $n = 3$ to 5). (D) HeLa cells expressing rtTA (control) or Rac1-V12G/Y40C were analyzed by Western blotting as described above with anti-Rac1 MAb. Molecular weight markers are indicated on the right. (E) HeLa cells expressing rtTA (control) or Rac1-V12G/Y40C were incubated with GFP-expressing A-MLV, Ad5, or VSV-pseudotyped lentivector overnight and analyzed as described above. Results are the percent infected cells normalized to values for rtTA control cells (means and SEM; $n = 3$). *, significantly different from the control.

cells, which exhibited a rounded or blunted shape with cortical F-actin deposition and a greatly diminished uptake of dextran, and Rac1-V12G cells, which assumed flattened cell profiles with broad peripheral lamellipodia and surface ruffles and were characterized by increased dextran uptake into a correspondingly increased number of macropinosomes per cell.

The effect of transgene expression on A-MLV infection was then analyzed by flow cytometry of GFP expression as described above. As seen in Fig. 7B, expression of Rac1-N17A inhibited while Rac1-V12G stimulated infection with A-MLV, while control cells expressing βSNC were not more or less susceptible to infection than NIH 3T3 rtTA control cells. RhoA marginally increased infection. Introduction of PAK1-K299A, the direct target of Rac1, inhibited A-MLV even more than Rac1-N17A itself, most likely due to differences in transgene expression levels (see Materials and Methods). As a control of presumed Rac1-V12G function specifically at the membrane, namely, recruitment to the subplasmalemma for actin modulation, we also confirmed that the effect of Rac1-V12G on A-MLV infection could be inhibited by EIPA and amiloride, but the 50 inhibitory concentration (IC_{50}) was increased (by a factor of 1.4) for both inhibitors in Rac1-V12G cells compared to control cells (Fig. 7C).

RhoG greatly increases macropinocytosis and A-MLV infectivity in HeLa cells. Human HeLa cells (cervical carcinoma derived) are efficiently transduced by VSV-pseudotyped lentivectors (reaching up to 90% of the total cell population), allowing more pure transgene-expressing cell populations to be obtained. To take advantage of this, and to expand our observations to other cell types than murine fibroblasts, we therefore also transduced HeLa rtTA cells with a panel of small GTPase mutants, including dominant negative RhoA-N19A, Rac1-N17A, and Cdc42-N17A, in addition to wild-type RhoG and dominant positive RhoG-Q61L and Rac1-V12G. Dominant active RhoG mutants have been described to increase macropinocytosis to an even higher degree than constitutively active Rac1 mutants (29). Because EIPA and amiloride exert their effect by preventing small-GTPase localization to the submembranous space, we considered that these drugs could potentially affect other small GTPases, such as RhoA and Cdc42, which regulate endocytosis through different clathrin- and caveolin-independent pathways (7).Therefore, we also included the dominant negative mutants RhoA-N19A and Cdc42-N17A.

All transgenes were expressed as proteins of the expected molecular weight (Fig. 8A). We next tested the effect of transgene expression on macropinocytosis of 70-kDa dextran in the HeLa cells (Fig. 8B). As expected, Rac1-V12G and RhoG both consistently increased macropinocytic uptake of dextran over the levels of HeLa rtTA control cells. However, surprisingly, Rac1-N17, which in NIH 3T3 efficiently blocked macropinocytosis, did not significantly affect macropinocytosis in HeLa cells for unknown reasons. Expression of RhoA-N19A and Cdc42-N17A did not cause altered macropinocytosis. We then examined the effect of transgene expression on A-MLV infection using lentivector pseudotyped with VSV-G as a control. While Rac1-V12G doubled the percentage of A-MLV-infected HeLa cells, we observed, in accor-

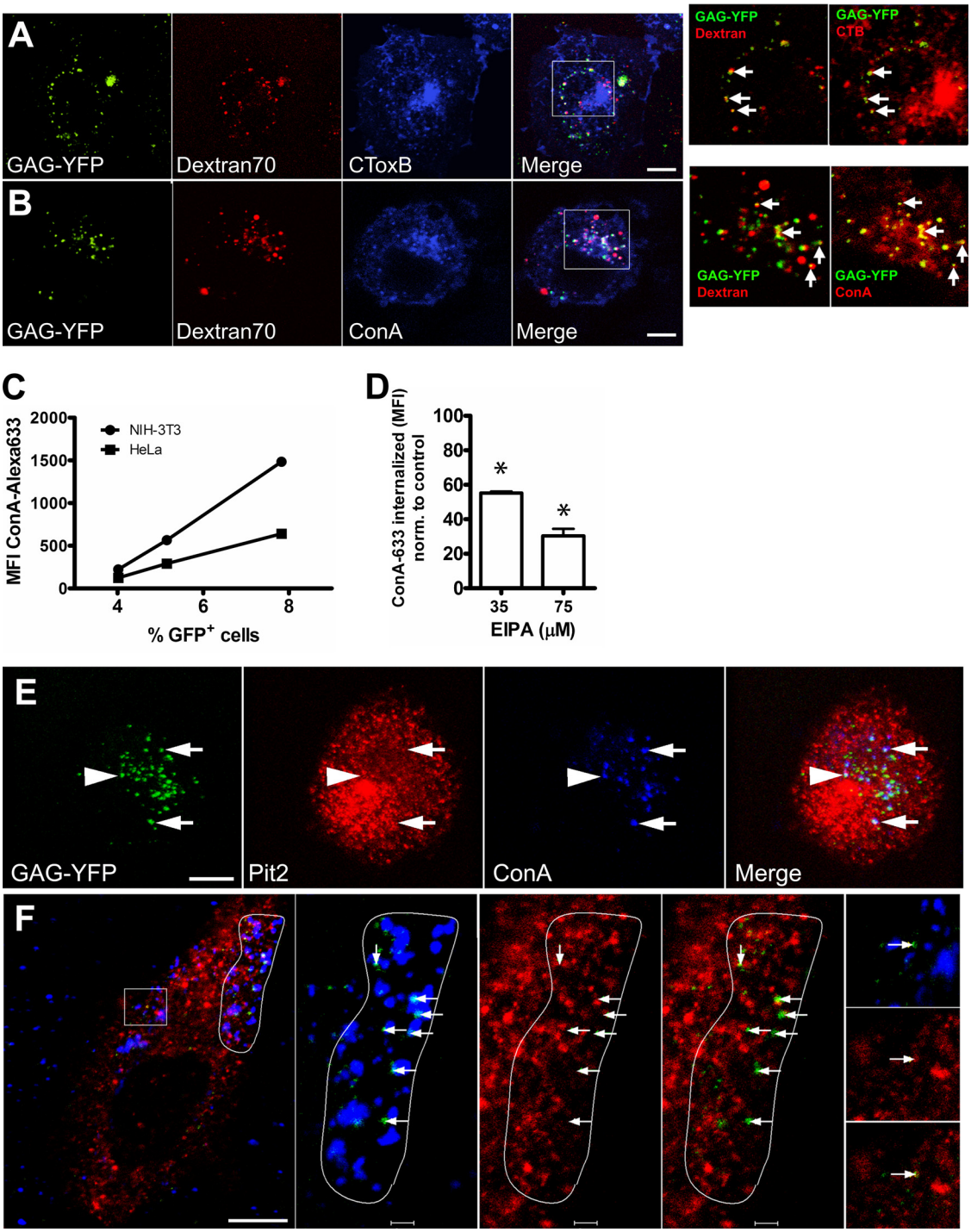

FIG 9 Internalized A-MLV is preferentially associated with macropinosomes and perinuclear vesicles following short internalization times. (A and B) HeLa cells expressing Rac1-V12G were incubated with A-MLV particles containing Gag-YFP and either Alexa 647-conjugated cholera toxin B subunit (CToxB) (A) or Alexa 647-conjugated ConA (B), both at 2.5 μg/ml at 4°C, before chase in the presence of TMR-conjugated 70-kDa dextran for 40 min at 37°C. Cells were subsequently imaged live at 20°C for up to 15 min by confocal microscopy. Note colocalization of Gag-YFP with dextran (A and B; arrows in first inset on right) and marked colocalization of these two markers with ConA (B; arrows in second inset) and to a lesser degree with CTB (A; second inset). Bars (A and B), 10 μm. (C) HeLa or NIH 3T3 cells were incubated with Alexa 647-conjugated ConA together with GFP-expressing A-MLV for 3 h at 37°C, washed, and then chased overnight. The next day, cells were analyzed for infection (GFP expression) and uptake of ConA by flow cytometry. The scatter diagram was divided into three gates corresponding to low, medium, and high levels of ConA uptake and correlated with the percentage of GFP-positive cells in each gate. The graph is representative of two independent experiments. (D) HeLa cells were incubated with Alexa 633-conjugated ConA for 2 h in the presence of EIPA before stringent washing and immediate flow-cytometric analysis of ConA uptake. Results are MFI of Alexa 633-conjugated ConA normalized to values for control untreated cells (means and SEM; $n = 3$). *, significantly different from the control. (E) HeLa cells were challenged with Gag-YFP-containing A-MLV (green) in the presence of Alexa 647-conjugated ConA (blue) for 1 h at 37°C and then processed for immunofluorescence with rabbit polyclonal anti-Pit2 antibodies (red). A single confocal plane from a *z* stack is shown to visualize individual A-MLV particles colocalizing with ConA in vacuoles also containing (arrows) or not (arrowhead)

dance with the lack of macropinocytic block, an insignificant effect of Rac1-N17A expression (Fig. 8C). Expression of dominant negative RhoA-N19A, as in NIH 3T3 cells, slightly stimulated infection of A-MLV, while Cdc42-N17A inhibited both A-MLV and lentivector infection by ca. 30%, perhaps reflecting a nonspecific effect on membrane trafficking. Notably, expression of both wild-type and dominant active RhoG-Q61L specifically increased A-MLV infection to levels of Rac1-V12G-expressing cells. Curious about the lack of effect of Rac1-N17A, we also tried expressing dominant positive PAK1-T423E (Fig. 8C). However, this mutant also did not significantly alter A-MLV infection. Despite this, introduction of the double mutant Rac1-V12G/Y40C, which has lost the ability to interact with and thereby activate PAK1, failed to replicate the increased A-MLV infection following Rac1-V12G expression (compare Fig. 8C with 8E), indicating that PAK1 interaction somehow is important for Rac1 function with respect to macropinocytosis and/or A-MLV infection.

A-MLV localizes to vacuolar structures enriched in concanavalin A binding sites. Finally, we sought to obtain a light-microscopic correlate of our observations. HeLa cells expressing Rac1-V12G (to increase the number of virions internalized) were incubated at 4°C with A-MLV and Alexa 647-conjugated CTB, which binds ganglioside GM1 in lipid rafts and caveolae, or Alexa 647-conjugated ConA. We conducted initial immunofluorescence studies to ensure that the concentrations of ConA used did not induce any clustering of cell surface proteins or domains (<8 μg/ml). After being washed, cells were chased at 37°C in the presence of TMR-conjugated 70-kDa dextran for 30 min followed by a washing before live observation at room temperature. As seen in Fig. 9A and B, A-MLV particles can be identified in vacuoles containing internalized 70-kDa dextran. A-MLV colocalization with CTB was present at low levels, but the colocalization with internalized ConA was pronounced (compare insets on the right in Fig. 9A and B), and many of these double-positive vacuoles contained 70-kDa dextran, indicating their macropinocytic origin. Although wheat germ agglutinin, another lectin, also showed colocalization with A-MLV, by far the best colocalization of all probes tested during the study was obtained for ConA. We therefore determined to what extent ConA uptake correlated with A-MLV uptake and macropinocytosis. As shown in Fig. 9F, there was a linear correlation between A-MLV infection and ConA uptake in individual cells, and further, cellular uptake of ConA in HeLa cells could be reduced to ca. 30% using 75 μM EIPA, indicating that a major fraction of internalized ConA derives from macropinocytosis. In fact, in many cell profiles, internalized A-MLV particles were found specifically concentrated in areas of cytosol with many ConA-positive macropinocytic vacuoles (Fig. 9F), and A-MLV virions were either contained within the vacuoles or closely juxtaposed, perhaps indicative of membrane fusion and escape of the capsid (containing the Gag-YFP moiety) into the cytosol. In a small subset of ConA-positive vacuoles containing A-MLV, it was also possible to see colocalization of Pit2 (Fig. 9E). A small, but consistent, fraction of A-MLV particles colocalized with caveolae on the cell surface (Fig. 9F, inset).

DISCUSSION

We show here that in contrast to previous claims (30) A-MLV does not depend on caveolae for endocytosis and infection. Instead, A-MLV enters via a macropinocytic mechanism requiring Na^+/H^+ exchange activity, actin dynamics, and the small GTPase Rac1 (or RhoG).

A-MLV does not depend on caveolae for entry. Caveolae are lipid raft-enriched flask-shaped invaginations of the plasma membrane (60 to 80 nm) which nicely accommodate a small naked or enveloped virus particle. Virus particles together with other multivalent ligands such as cholera toxin, which induce protein and/or lipid aggregation and stabilize the liquid-ordered phase of cell surface lipids, can indeed be localized to caveolae in some instances (45). This fact has misled several groups in the past to conclude that caveolae also constitute the main portal of entry for viruses such as SV40 (45) and toxins such as cholera toxin. However, when essentially the same experiments were carried out in caveolin-null MEFs, it could be concluded that caveolae played an insignificant or even slightly inhibitory role in the endocytosis of these ligands (16, 37). Rather, both SV40 and cholera toxin, which share the cellular GM1 receptor, are internalized by (different) clathrin- and caveolin-independent endocytosis mechanisms (16, 37). The authors of the original study (30) based their assumption of caveolar entry on nonspecific methods of manipulation of caveolae and a failure to consider and experimentally exclude other potential pathways of internalization. In addition, we find that the great majority of Pit2 is TX-100 soluble and therefore not present in lipid rafts.

In the present study, we used caveolin-1-null MEFs and shRNA knockdown NIH 3T3 cells to show that absence of caveolae does not interfere with A-MLV internalization and infection. Along these lines, a deficiency of dynamin, which is required for caveolar budding from the membrane, in knockout MEFs did not impede virus uptake, and more importantly, overexpression of dominant negative dynamin in HeLa cells only moderately decreased A-MLV infection while markedly inhibiting Ad5 infection, which served as a control. In fact, in the presence of Polybrene, which increases virus particle binding to the cell surface, we observed caveolae to be an impeding factor for A-MLV infection in wild-type MEFs. This is in agreement with previous findings showing that the presence of caveolae restrains SV40 endocytosis and infection in wild-type compared to caveolin-1-null MEFs (16), likely due to the relative inertness of caveolae with regard to endocytosis (10). Consistent with such an interpretation, we did observe a low degree of colocalization between caveolae and A-MLV on the cell surface by immunofluorescence.

A-MLV entry via macropinocytosis. A small number of viruses (<10) are known to become internalized by different forms of macropinocytosis (8, 24), and the data presented here indicate that A-MLV should be added to this list. First, our electron-microscopic (EM) and light-microscopic observations show that A-MLV virions are present in cell surface areas engaged in extensive ruffling and vacuole formation, and A-MLV particles could be

containing Pit2. Bar, 10 μm. (F) HeLa cells were incubated with Gag-YFP-containing A-MLV (green) in the presence of Alexa 647-conjugated ConA (blue) at 4°C and then chased for 1 h at 37°C before fixation for immunofluorescence with rabbit polyclonal anti-caveolin-1 antibodies (red). Note that the great majority of internalized A-MLV is present in cortical areas close to segments of plasma membrane with high macropinocytic activity (white outline on right) where virus particles are found in or next to ConA-labeled macropinosomes (arrows). In contrast, A-MLV colocalization with caveolin-1 is observable only at low frequency on the cell surface (boxed area; arrows in insets at far right). Bars, 10 μm and 2 μm (insets).

localized to the lumen of 70-kDa-dextran-containing vacuoles, indicative of macropinosomes. Second, inhibition of Na^+/H^+ exchange activity with low concentrations of EIPA or amiloride specifically blocked infection by A-MLV but not other virus types internalized by clathrin-coated-pit endocytosis. The same specific inhibition of A-MLV infection was also true of F-actin depolymerization with latrunculin or cytochalasin D. Third, we show that introduction of dominant positive mutants of the small GTPases Rac1 and RhoG, which increase macropinocytosis, also cause a corresponding increase in A-MLV infection. Finally, we show by the introduction of dominant negative dynamin-1-K44A, RhoA, and Cdc42 that clathrin-mediated or RhoA- or Cdc42-regulated clathrin- and caveolin-independent pathways (39, 46), respectively, that could potentially work concurrently with macropinocytosis in surface areas with membrane ruffling do not contribute to A-MLV uptake and infection. Importantly, we also demonstrate by okadaic acid- or suspension-stimulated caveolae endocytosis that A-MLV entry can be uncoupled from caveolae internalization with respect to uptake and infection, and it is therefore unlikely that A-MLV changes its normal uptake route from caveolae to macropinocytosis in the absence of the former.

As controls of specificity, we used E-MLV, Ad5, and VSV-G-pseudotyped lentivirus. While the entry route of E-MLV remains to be determined (43), both Ad5 and VSV-G (41) are internalized through clathrin-coated pits. Ad2 and Ad5 are both internalized via the same receptor complex of coxsackievirus and adenovirus receptor (CAR) and integrins, which traffic through clathrin-coated pits (42, 47). It is therefore assumed that Ad5, like Ad2, depends on concurrent macropinocytosis to allow escape of virus from endosomes by their lysis (47), and it has been reported that 100 μM EIPA inhibits Ad5 infection in HeLa cells (47). Note, however, that pathogens and toxins that use the same cell surface receptor do not necessarily traffic in an identical manner (16, 37), and conversely, closely related vaccinia virus strains that present the same envelope cell surface-binding antigen (phosphatidylserine) internalize through different mechanisms of macropinocytosis (48).

In addition, at least in our hands, such relatively high EIPA concentrations also adversely affect clathrin-coated-pit endocytosis in HeLa cells. In the present study, 35 to 50 μM EIPA inhibited A-MLV infection by up to 85%, while entry and infection of VSV and Ad5 were not inhibited. We speculate that if Ad5 requires macropinosome formation for endosomal lysis and viral escape, an incomplete block of macropinocytosis at the lower (specific) concentrations of EIPA used here allows Ad5 escape (as a catalytic mechanism), while A-MLV infection, which depends on macropinocytosis as the direct physical entry mechanism, is severely blocked.

Different mechanisms of macropinosome formation are observed in cells under physiological conditions or following virus or pathogen exposure, including lamellipodial ruffles and circular ruffles (in addition to filopodial and blebbing macropinocytosis) (24).

Lamellipodial ruffles are formed at the periphery and depend on Rac1 and PAK1 for both ruffling and macropinosome closure (49), whereas circular ruffles have a less stringent requirement for PAK1 and maybe even Rac1, and macropinosome scission occurs through dynamin activity (49–51). Activation of Rac1 is sufficient to drive macropinocytosis (44), and we observe that introduction of Rac1-V12G in both NIH 3T3 and HeLa cells increase macropinocytosis and A-MLV infection. In contrast, whereas dominant negative Rac1-N17A and PAK1-K299A blocked macropinocytosis and A-MLV infection in NIH 3T3 cells as expected, this inhibitory effect was absent in HeLa cells, which also did not respond to expression of dominant positive PAK1-T423E, reported to increase macropinocytosis (27). Nevertheless, A-MLV infection in HeLa cells expressing Rac1-V12G/Y40C, deficient in PAK binding and activation, was not increased. The effect of Rac1-V12G therefore requires PAK1, but likely not in a classical manner.

Both RhoG and its GTP SH3-containing guanine nucleotide exchange factor (SGEF) provoke the formation of circular dorsal ruffles and macropinocytosis (29). Although RhoG can activate Rac1 through regulation of GTP exchange factors of Rac1 (52), cells expressing SGEF do not show an increase in active, GTP-loaded Rac1 (29), and it is presently unknown how RhoG promotes macropinocytosis. Since RhoG and dominant positive RhoG-Q61L increased macropinocytosis and A-MLV infection to the same extent as Rac1-V12G, our data indicate that A-MLV infection, at least in HeLa cells, can occur through macropinosomes formed from both lamellipodial and circular ruffles. Along these lines, closely related strains of vaccinia virus can use different forms of macropinocytosis to gain cell entry by differential activation of Rac1 and Cdc42 GTPases (48). The 30% decrease in A-MLV infection following expression of dynamin-1-K44A that we observed could therefore to a degree reflect A-MLV entry through macropinosomes formed from circular ruffles, which require dynamin function.

ACKNOWLEDGMENTS

We are indebted to Wayne Anderson, Laboratory of Cellular Oncology, National Cancer Institute, NIH, USA, for the generous contribution of Pit2-related vectors and antibodies. We greatly appreciate the expert help of Mette Ohlsen with cryo-EM and the help of graduate students Zvezdana Moneva and Biljana Mojsoska in preparatory phases of this work.

There are no conflicts of interest to declare.

This study was supported by a grant to F.V. from the Lundbeck Foundation (R67-A6520).

REFERENCES

1. **Feldman SA, Farrell KB, Murthy RK, Russ JL, Eiden MV.** 2004. Identification of an extracellular domain within the human PiT2 receptor that is required for amphotropic murine leukemia virus binding. J Virol **78:** 595–602. http://dx.doi.org/10.1128/JVI.78.2.595-602.2004.
2. **van Zeijl M, Johann SV, Closs E, Cunningham J, Eddy R, Shows TB, O'Hara B.** 1994. A human amphotropic retrovirus receptor is a second member of the gibbon ape leukemia virus receptor family. Proc Natl Acad Sci U S A **91:**1168–1172. http://dx.doi.org/10.1073/pnas.91.3.1168.
3. **Walker SJ, Pizzato M, Takeuchi Y, Devereux S.** 2002. Heparin binds to murine leukemia virus and inhibits Env-independent attachment and infection. J Virol **76:**6909–6918. http://dx.doi.org/10.1128/JVI.76.14.6909-6918.2002.
4. **Beer C, Pedersen L.** 2007. Matrix fibronectin binds gammaretrovirus and assists in entry: new light on viral infections. J Virol **81:**8247–8257. http://dx.doi.org/10.1128/JVI.00312-07.
5. **Jobbagy Z, Garfield S, Baptiste L, Eiden MV, Anderson WB.** 2000. Subcellular redistribution of Pit-2 P(i) transporter/amphotropic leukemia virus (A-MuLV) receptor in A-MuLV-infected NIH 3T3 fibroblasts: involvement in superinfection interference. J Virol **74:**2847–2854. http://dx.doi.org/10.1128/JVI.74.6.2847-2854.2000.
6. **Rodrigues P, Heard JM.** 1999. Modulation of phosphate uptake and amphotropic murine leukemia virus entry by posttranslational modifications of PIT-2. J Virol **73:**3789–3799.
7. **Kirkham M, Parton RG.** 2005. Clathrin-independent endocytosis: new in-

sights into caveolae and non-caveolar lipid raft carriers. Biochim Biophys Acta **1746:**349–363. http://dx.doi.org/10.1016/j.bbamcr.2005.11.005.
8. **Mercer J, Helenius A.** 2009. Virus entry by macropinocytosis. Nat Cell Biol **11:**510–520. http://dx.doi.org/10.1038/ncb0509-510.
9. **Marsh M, Helenius A.** 2006. Virus entry: open sesame. Cell **124:**729–740. http://dx.doi.org/10.1016/j.cell.2006.02.007.
10. **Hommelgaard AM, Roepstorff K, Vilhardt F, Torgersen ML, Sandvig K, van Deurs B.** 2005. Caveolae: stable membrane domains with a potential for internalization. Traffic **6:**720–724. http://dx.doi.org/10.1111/j.1600-0854.2005.00314.x.
11. **Boucrot E, Howes MT, Kirchhausen T, Parton RG.** 2011. Redistribution of caveolae during mitosis. J Cell Sci **124:**1965–1972. http://dx.doi.org/10.1242/jcs.076570.
12. **Choudhury A, Marks DL, Proctor KM, Gould GW, Pagano RE.** 2006. Regulation of caveolar endocytosis by syntaxin 6-dependent delivery of membrane components to the cell surface. Nat Cell Biol **8:**317–328. http://dx.doi.org/10.1038/ncb1380.
13. **Moren B, Shah C, Howes MT, Schieber NL, McMahon HT, Parton RG, Daumke O, Lundmark R.** 2012. EHD2 regulates caveolar dynamics via ATP-driven targeting and oligomerization. Mol Biol Cell **23:**1316–1329. http://dx.doi.org/10.1091/mbc.E11-09-0787.
14. **Pelkmans L, Burli T, Zerial M, Helenius A.** 2004. Caveolin-stabilized membrane domains as multifunctional transport and sorting devices in endocytic membrane traffic. Cell **118:**767–780. http://dx.doi.org/10.1016/j.cell.2004.09.003.
15. **Nichols B.** 2003. Caveosomes and endocytosis of lipid rafts. J Cell Sci **116:**4707–4714. http://dx.doi.org/10.1242/jcs.00840.
16. **Damm EM, Pelkmans L, Kartenbeck J, Mezzacasa A, Kurzchalia T, Helenius A.** 2005. Clathrin- and caveolin-1-independent endocytosis: entry of simian virus 40 into cells devoid of caveolae. J Cell Biol **168:**477–488. http://dx.doi.org/10.1083/jcb.200407113.
17. **Amstutz B, Gastaldelli M, Kalin S, Imelli N, Boucke K, Wandeler E, Mercer J, Hemmi S, Greber UF.** 2008. Subversion of CtBP1-controlled macropinocytosis by human adenovirus serotype 3. EMBO J **27:**956–969. http://dx.doi.org/10.1038/emboj.2008.38.
18. **Pernet O, Pohl C, Ainouze M, Kweder H, Buckland R.** 2009. Nipah virus entry can occur by macropinocytosis. Virology **395:**298–311. http://dx.doi.org/10.1016/j.virol.2009.09.016.
19. **Raghu H, Sharma-Walia N, Veettil MV, Sadagopan S, Chandran B.** 2009. Kaposi's sarcoma-associated herpesvirus utilizes an actin polymerization-dependent macropinocytic pathway to enter human dermal microvascular endothelial and human umbilical vein endothelial cells. J Virol **83:**4895–4911. http://dx.doi.org/10.1128/JVI.02498-08.
20. **Saeed MF, Kolokoltsov AA, Albrecht T, Davey RA.** 2010. Cellular entry of Ebola virus involves uptake by a macropinocytosis-like mechanism and subsequent trafficking through early and late endosomes. PLoS Pathog 6:e1001110. http://dx.doi.org/10.1371/journal.ppat.1001110.
21. **Nanbo A, Imai M, Watanabe S, Noda T, Takahashi K, Neumann G, Halfmann P, Kawaoka Y.** 2010. Ebolavirus is internalized into host cells via macropinocytosis in a viral glycoprotein-dependent manner. PLoS Pathog **6:**e1001121. http://dx.doi.org/10.1371/journal.ppat.1001121.
22. **Kalin S, Amstutz B, Gastaldelli M, Wolfrum N, Boucke K, Havenga M, DiGennaro F, Liska N, Hemmi S, Greber UF.** 2010. Macropinocytotic uptake and infection of human epithelial cells with species B2 adenovirus type 35. J Virol **84:**5336–5350. http://dx.doi.org/10.1128/JVI.02494-09.
23. **Gold S, Monaghan P, Mertens P, Jackson T.** 2010. A clathrin independent macropinocytosis-like entry mechanism used by bluetongue virus-1 during infection of BHK cells. PLoS One **5:**e11360. http://dx.doi.org/10.1371/journal.pone.0011360.
24. **Mercer J, Helenius A.** 2012. Gulping rather than sipping: macropinocytosis as a way of virus entry. Curr Opin Microbiol **15:**490–499. http://dx.doi.org/10.1016/j.mib.2012.05.016.
25. **Swanson JA.** 2008. Shaping cups into phagosomes and macropinosomes. Nat Rev Mol Cell Biol **9:**639–649. http://dx.doi.org/10.1038/nrm2447.
26. **Koivusalo M, Welch C, Hayashi H, Scott CC, Kim M, Alexander T, Touret N, Hahn KM, Grinstein S.** 2010. Amiloride inhibits macropinocytosis by lowering submembranous pH and preventing Rac1 and Cdc42 signaling. J Cell Biol **188:**547–563. http://dx.doi.org/10.1083/jcb.200908086.
27. **Dharmawardhane S, Schurmann A, Sells MA, Chernoff J, Schmid SL, Bokoch GM.** 2000. Regulation of macropinocytosis by p21-activated kinase-1. Mol Biol Cell **11:**3341–3352. http://dx.doi.org/10.1091/mbc.11.10.3341.
28. **Liberali P, Kakkonen E, Turacchio G, Valente C, Spaar A, Perinetti G, Bockmann RA, Corda D, Colanzi A, Marjomaki V, Luini A.** 2008. The closure of Pak1-dependent macropinosomes requires the phosphorylation of CtBP1/BARS. EMBO J **27:**970–981. http://dx.doi.org/10.1038/emboj.2008.59.
29. **Ellerbroek SM, Wennerberg K, Arthur WT, Dunty JM, Bowman DR, DeMali KA, Der C, Burridge K.** 2004. SGEF, a RhoG guanine nucleotide exchange factor that stimulates macropinocytosis. Mol Biol Cell **15:**3309–3319. http://dx.doi.org/10.1091/mbc.E04-02-0146.
30. **Beer C, Andersen DS, Rojek A, Pedersen L.** 2005. Caveola-dependent endocytic entry of amphotropic murine leukemia virus. J Virol **79:**10776–10787. http://dx.doi.org/10.1128/JVI.79.16.10776-10787.2005.
31. **Razani B, Engelman JA, Wang XB, Schubert W, Zhang XL, Marks CB, Macaluso F, Russell RG, Li M, Pestell RG, Di Vizio D, Hou H, Jr, Kneitz B, Lagaud G, Christ GJ, Edelmann W, Lisanti MP.** 2001. Caveolin-1 null mice are viable but show evidence of hyperproliferative and vascular abnormalities. J Biol Chem **276:**38121–38138.
32. **Andrawiss M, Takeuchi Y, Hewlett L, Collins M.** 2003. Murine leukemia virus particle assembly quantitated by fluorescence microscopy: role of Gag-Gag interactions and membrane association. J Virol **77:**11651–11660. http://dx.doi.org/10.1128/JVI.77.21.11651-11660.2003.
33. **Roepstorff K, Rasmussen I, Sawada M, Cudre-Maroux C, Salmon P, Bokoch G, van Deurs B, Vilhardt F.** 2008. Stimulus-dependent regulation of the phagocyte NADPH oxidase by a VAV1, Rac1, and PAK1 signaling axis. J Biol Chem **283:**7983–7993. http://dx.doi.org/10.1074/jbc.M708281200.
34. **Vilhardt F, Nielsen M, Sandvig K, van Deurs B.** 1999. Urokinase-type plasminogen activator receptor is internalized by different mechanisms in polarized and nonpolarized Madin-Darby canine kidney epithelial cells. Mol Biol Cell **10:**179–195. http://dx.doi.org/10.1091/mbc.10.1.179.
35. **Fra AM, Williamson E, Simons K, Parton RG.** 1995. De novo formation of caveolae in lymphocytes by expression of VIP21-caveolin. Proc Natl Acad Sci U S A **92:**8655–8659. http://dx.doi.org/10.1073/pnas.92.19.8655.
36. **Parton RG, Joggerst B, Simons K.** 1994. Regulated internalization of caveolae. J Cell Biol **127:**1199–1215. http://dx.doi.org/10.1083/jcb.127.5.1199.
37. **Kirkham M, Fujita A, Chadda R, Nixon SJ, Kurzchalia TV, Sharma DK, Pagano RE, Hancock JF, Mayor S, Parton RG.** 2005. Ultrastructural identification of uncoated caveolin-independent early endocytic vehicles. J Cell Biol **168:**465–476. http://dx.doi.org/10.1083/jcb.200407078.
38. **Balasubramanian N, Scott DW, Castle JD, Casanova JE, Schwartz MA.** 2007. Arf6 and microtubules in adhesion-dependent trafficking of lipid rafts. Nat Cell Biol **9:**1381–1391. http://dx.doi.org/10.1038/ncb1657.
39. **Howes MT, Mayor S, Parton RG.** 2010. Molecules, mechanisms, and cellular roles of clathrin-independent endocytosis. Curr Opin Cell Biol **22:**519–527. http://dx.doi.org/10.1016/j.ceb.2010.04.001.
40. **Damke H, Baba T, Warnock DE, Schmid SL.** 1994. Induction of mutant dynamin specifically blocks endocytic coated vesicle formation. J Cell Biol **127:**915–934. http://dx.doi.org/10.1083/jcb.127.4.915.
41. **Finkelshtein D, Werman A, Novick D, Barak S, Rubinstein M.** 2013. LDL receptor and its family members serve as the cellular receptors for vesicular stomatitis virus. Proc Natl Acad Sci U S A **110:**7306–7311. http://dx.doi.org/10.1073/pnas.1214441110.
42. **Gastaldelli M, Imelli N, Boucke K, Amstutz B, Meier O, Greber UF.** 2008. Infectious adenovirus type 2 transport through early but not late endosomes. Traffic **9:**2265–2278. http://dx.doi.org/10.1111/j.1600-0854.2008.00835.x.
43. **Lee S, Zhao Y, Anderson WF.** 1999. Receptor-mediated Moloney murine leukemia virus entry can occur independently of the clathrin-coated-pit-mediated endocytic pathway. J Virol **73:**5994–6005.
44. **Fujii M, Kawai K, Egami Y, Araki N.** 2013. Dissecting the roles of Rac1 activation and deactivation in macropinocytosis using microscopic photo-manipulation. Sci Rep **3:**2385. http://dx.doi.org/10.1038/srep02385.
45. **Pelkmans L, Kartenbeck J, Helenius A.** 2001. Caveolar endocytosis of simian virus 40 reveals a new two-step vesicular-transport pathway to the ER. Nat Cell Biol **3:**473–483. http://dx.doi.org/10.1038/35074539.
46. **Doherty GJ, McMahon HT.** 2009. Mechanisms of endocytosis. Annu Rev Biochem **78:**857–902. http://dx.doi.org/10.1146/annurev.biochem.78.081307.110540.
47. **Meier O, Boucke K, Hammer SV, Keller S, Stidwill RP, Hemmi S, Greber UF.** 2002. Adenovirus triggers macropinocytosis and endosomal

leakage together with its clathrin-mediated uptake. J Cell Biol **158:**1119–1131. http://dx.doi.org/10.1083/jcb.200112067.

48. **Mercer J, Knebel S, Schmidt FI, Crouse J, Burkard C, Helenius A.** 2010. Vaccinia virus strains use distinct forms of macropinocytosis for host-cell entry. Proc Natl Acad Sci U S A **107:**9346–9351. http://dx.doi.org/10.1073/pnas.1004618107.
49. **Hoon JL, Wong WK, Koh CG.** 2012. Functions and regulation of circular dorsal ruffles. Mol Cell Biol **32:**4246–4257. http://dx.doi.org/10.1128/MCB.00551-12.
50. **Schlunck G, Damke H, Kiosses WB, Rusk N, Symons MH, Waterman-Storer CM, Schmid SL, Schwartz MA.** 2004. Modulation of Rac localization and function by dynamin. Mol Biol Cell **15:**256–267. http://dx.doi.org/10.1091/mbc.E03-01-0019.
51. **Liu YW, Surka MC, Schroeter T, Lukiyanchuk V, Schmid SL.** 2008. Isoform and splice-variant specific functions of dynamin-2 revealed by analysis of conditional knock-out cells. Mol Biol Cell **19:**5347–5359. http://dx.doi.org/10.1091/mbc.E08-08-0890.
52. **Katoh H, Negishi M.** 2003. RhoG activates Rac1 by direct interaction with the Dock180-binding protein Elmo. Nature **424:**461–464. http://dx.doi.org/10.1038/nature01817.